

# Measurement-Based Thermal Modeling Using Laser Thermography

Tamas Aujeszky, Georgios Korres, and Mohamad Eid

**Abstract**—There have been several studies in using infrared thermography for nondestructive evaluation and testing of materials. Some studies have explored the potential of using thermography for classification of materials based on their thermal response. However, the modeling behind these efforts is rather simplistic, and in some ways not corresponding well with practical applications. This paper presents a realistic model-based approach for characterizing unknown materials using laser thermography. The process being modeled is laser excitation step thermography with finite but not infinitesimal excitation length and uniform distribution over a finite radius. A mathematical model, based on the heat equation that governs the flow of heat in materials, is introduced to characterize objects based on their response to thermal excitation. Experimental results consistently demonstrated the ability of the proposed approach to classify different materials based on their thermal properties. This contactless characterization method might prove to be suitable for a range of applications including teleoperation, haptic mapping and multimodal human computer interaction.

**Index Terms**—Infrared imaging, haptic interfaces, mathematical model, measurement by laser beam, thermal variables measurement.

## I. INTRODUCTION

MODERN 3-D scanning is becoming a mature practice for the acquisition of the geometry of objects. However, capturing the thermal and physical properties of objects is required to create precise and realistic physical interactions. For instance, in teleoperation applications, accurate thermal/physical interactions can be simulated given the thermal/physical properties of the environment. The need to scan the thermal/physical properties of objects is highlighted by the emergence of haptic rendering (including force feedback and thermal rendering), haptic/thermal display technologies, and multimodal human–computer interaction.

Haptic technologies have traditionally dealt with tactile and kinesthetic feedback to a human operator. Thermal interaction occurring between the fingertip and an explored surface plays a prominent role in the tactile exploration [1]. Furthermore, thermal interaction between the user and an explored surface

is crucial when visual information is limited, or when a more realistic image of the object is required [2]. The existing research has focused on rendering thermal interactions with virtual environments (thermal display and thermal rendering algorithms). However, mapping objects based on their thermal response is not as well explored.

The purpose of this paper is to develop a novel approach for thermal modeling using laser thermography in order to enable thermal interactions with the modeled material. A mathematical model, based on the heat equation, is developed to describe the phenomenon of thermal diffusion and correlations to the thermal properties of the material. The presented model is first verified by simulation and then an experiment is conducted to demonstrate the usability of this approach in classifying objects of different materials.

The rest of this paper is organized as follows. Section II presents an overview of the related work in this field, while Section III outlines the mathematical model. Section IV contains simulations based on the model to ascertain its level of realism, and Section V presents an experimental study for classifying multiple materials, as well as a discussion about the results. Finally, Section VI summarizes the conclusion and discusses the future work. The detailed mathematical derivation of the model can be found in the Appendix.

## II. RELATED WORK

### A. Infrared Thermography

Infrared thermography uses the heat signature of an object to derive information about the properties of the object (thermal, mechanical, or electrical) [3], [4]. Thermographic inspections have been used as a tool for industrial testing since as early as the 1980s [5]–[14]. Over the past decades, thermography has also been used as a tool in submicrometer electronic circuits, with applications such as finding leakage current [15] or characterizing the thermal behavior of circuit components [16], [17]. Due to its contactless and nondestructive properties, infrared thermography is also one of the preferred techniques in use for examining works of art [18]–[21]. Currently, the field encompasses many different use case scenarios, as presented in a detailed review by Usamentiaga *et al.* [22].

Infrared thermography is categorized as either passive or active. Passive thermography measures properties that have a naturally different temperature than their surroundings or a naturally occurring thermal gradient. Active thermography utilizes an energy source to create a thermal contrast within the object under examination, whose evolution over time and space can then be assessed in order to obtain characteristic

Manuscript received July 15, 2017; revised September 4, 2017; accepted October 13, 2017. Date of publication February 28, 2018; date of current version May 10, 2018. The Associate Editor coordinating the review process was Dr. V. R. Singh. (Corresponding author: Mohamad Eid.)

T. Aujeszky is with the Department of Electrical Engineering, New York University Abu Dhabi, Abu Dhabi 129188, United Arab Emirates.

G. Korres is with New York University Abu Dhabi, Abu Dhabi 129188, United Arab Emirates.

M. Eid is with the Department of Electrical and Computer Engineering, New York University Abu Dhabi, Abu Dhabi 129188, United Arab Emirates (e-mail: mohamad.eid@nyu.edu).

Color versions of one or more of the figures in this paper are available online at <http://ieeexplore.ieee.org>.

Digital Object Identifier 10.1109/TIM.2017.2785138

0018-9456 © 2018 IEEE. Personal use is permitted, but republication/redistribution requires IEEE permission.  
See [http://www.ieee.org/publications\\_standards/publications/rights/index.html](http://www.ieee.org/publications_standards/publications/rights/index.html) for more information.

information about the object. This information is related to thermal diffusivity, a fundamental characteristic property of any material that measures its ability to conduct heat as opposed to storing it. Estimating thermal diffusivity through infrared thermography is a popular direction of research [23]–[29], however, most existing publications rely on a somewhat restrictive and not entirely lifelike model that provides a closed form equation for thermal diffusivity. This is due to the fact that this model assumes instantaneous energy transfer from a heat source with the Gaussian distribution of intensity, which is also assumed to be directly mapped as such on the surface of the object. Excitation for active thermography can take place in mechanical, electromagnetic, or optical forms, which represent separate branches of the field. Infrared thermography seems to overcome the need for physical contact between the measurement tool and the object surface. Furthermore, it has the potential to generate haptic models in soft real-time fashion. Therefore, this approach seems promising for haptic modeling.

### B. Thermal Modeling

Thermal modeling has been applied in various fields (automotive electronic devices [37], defect detection in cement-based material [38], inspection of composite materials [39], measuring thickness of coatings on metallic surfaces [40], and among others). One interesting application for thermal modeling is to simulate realistic interaction between the human and a touched object in virtual reality. For example, thermal cues have been shown to be effective in facilitating the identification and discrimination of objects in virtual environments [41].

Previous work on human thermal interaction (perception and psychophysical mechanisms involved during touch exploration) focused on developing thermal interfaces and thermal rendering software [30]. A thermal interface typically consists of thermal stimulator(s), thermal sensor(s), and a temperature control system that monitors and controls the surface temperature of the thermal interface [33]–[36]. Thermal rendering involves the computation required to determine heat transfer between the skin and the touched object in order to simulate realistic thermal interactions. Modeling such interaction is complicated, involving factors from the human side (such as skin temperature, skin surface properties, and blood perfusion) as well as the object side (object temperature, object material properties, geometry, and texture).

A number of thermal models have been developed to characterize the thermal interaction between the skin and an object during touch, with various assumptions about the directionality of temperature variation, the presence of thermal contact resistance, and the contribution of metabolic heat generation and blood perfusion to the thermal responses [31] [42]–[46]. For instance, Jones and Ho [31] encoded thermal stimulation as being warm or cool, and then quantified the corresponding thermal stimulation in terms of intensity and duration.

A potential application for thermal modeling is automatic material characterization and/or identification in robotics applications. Bhattacharjee *et al.* [32] focus on material

recognition from heat transfer given varying initial conditions, short-duration contact, and ambient temperature. Results confirmed the feasibility of material classification by robots based on measurements acquired during short-duration contact. This clearly requires a physical contact between the robot and the material surface.

### C. Summary

It can be seen from the previous sections that there is interest in the field for developing systems that perform material recognition, classification, or characterization by performing active thermography. Although thermography has been used for decades in various industries, the primary usage has been for nondestructive, qualitative evaluation, and testing. The existing approaches relied on a closed-form equation for thermal diffusivity that is correct only with certain assumptions (i.e. the source has a Gaussian distribution that is directly and instantaneously mapped onto the surface). Our work uses a general approach where the distribution can be specified—for our experiment, we used a uniform disk-shaped distribution model that corresponds well with the laser source. Additionally, our approach is not flash, but step thermography, where the excitation energy is supplied over a measurable amount of time. This makes it more suitable for delicate materials than flash thermography, where all the energy hits the material in an instant. Additionally, it is more correct to model even flash excitation as lasting for a period of time rather than an instant, which is impractical.

The aim of this paper is to propose a thermal model for laser excitation step thermography and demonstrate its potential for the classification of different materials. This model enables a method for material characterization that is contactless and nondestructive, making possible physical interaction between a robot and its environment even if it consists of delicate objects. Noncontact measurement removes the need to apply a contact force on the material, thereby, preserving delicate samples. In addition, given good resolution and sufficient power, a noncontact measurement can be done via a larger distance range than contact measurements, which need direct physical connection to the object. As such, noncontact measurements can be simultaneously conducted on objects at different distances, without a need to reposition the measurement system, or the objects in question. This is especially important for teleoperation applications.

## III. MODELING

The basis of the model is the well-known heat equation: a second-order differential equation [45] that describes the relationship between the spatial distribution and the temporal evolution of heat. In order to find the unique solution to the heat equation that directly corresponds to the thermography procedure, we need to specify a set of conditions that can be viewed as a fair approximation of reality. The model is based on the following assumptions.

- 1) The sample is treated as an infinite 2-D slice of space with finite thickness.

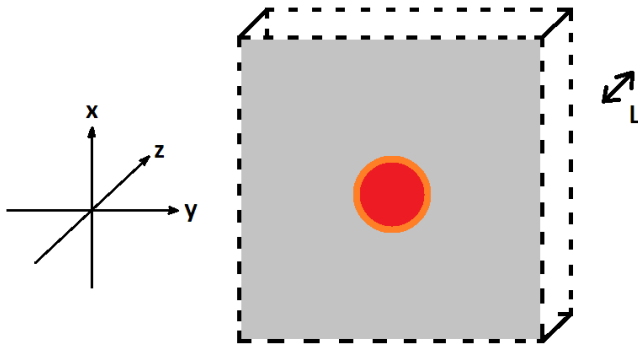


Fig. 1. Diagram of the modeled scenario, with the center of excitation taken as the origin.

- 2) The sample is treated as composed of a single homogeneous material.
- 3) We assume that no heat flow is present through the surface boundaries of the material except for the laser source.
- 4) The sample is assumed to be initially (before the laser diode is turned on) at ambient temperature and in thermal equilibrium with itself.
- 5) We treat the source as homogeneously acting in a finite but nonzero radius of incidence and over a finite but nonzero amount of time.

Fig. 1 represents a diagram of the modeled scenario. The mathematical formulation of the above assumptions is contained in the following sections, while the derivation of the heat equation is included in the Appendix.

*A. Base Conditions*

In order to formulate a realistic mathematical model, we have to make several general assumptions that are stated here. First, the sample is treated as an infinite slice of space with known thickness  $L$ . This is a valid abstraction of real-life objects with a large enough surface area that a heat source at the center causes negligible heating at the surface edges over a short period of time. A 3-D Cartesian coordinate system is used, as such: the object is aligned parallel to the  $xy$  plane, such that its boundaries are at  $z = 0$  and  $z = L$ . The center of the laser excitation will take place at the origin, meaning that the laser source and the thermal camera are at the  $z = 0$  side of the sample. These conditions are illustrated by Fig. 1.

In addition to the above abstractions, we are also assuming that the sample material is homogeneous with respect to its thermal properties: thermal conductivity and volumetric heat capacity (with thermal diffusivity being the ratio of these two properties).

*B. Boundary Conditions*

The following boundary conditions are applied. As is the case with dimensions without a mathematical boundary, in the  $x$ - and  $y$ -directions the boundary condition is that the solution has to be bounded in amplitude.

For the  $z$ -direction, it is an aim to find a solution that corresponds to no heat exchange at the boundary. This is given

by the Neumann boundary condition, stating  $\partial T / \partial z = 0$  at  $z = 0$  and  $z = L$ . There are multiple ways to account for this condition, but the most convenient one is the method of images. It involves a symmetrical extension of the problem around  $z = 0$ , thereby ensuring that the differential of the temperature will always be 0 at  $z = 0$ . This is due to the property of the heat equation that regardless of the initial conditions, the temperature function becomes a smooth function for any  $t > 0$ . However, it also needs to be ensured that the same symmetric extension is applied around  $z = L$  in order to uphold the same boundary condition at that location. The only way to uphold both symmetries is by mirroring the original problem infinitely many times outward in both directions, so that in the end the problem becomes infinite in the  $z$ -direction as well, with mirrored initial conditions and mirrored (image) sources. This model neglects the effects of advective heat currents at the surface of the object in reality. The reason for this is that the magnitude of this effect is in fact negligible under most sets of conditions, as visible in Section V-D for the experiment.

*C. Initial Conditions*

For the initial condition, we assume that the object initially is in thermal equilibrium with its surroundings at a temperature denoted by  $T_0$ . As visible from the results in the Appendix,  $T_0$  is only manifested as an added constant term in the final equations. Therefore, in simulation, it is logical to consider the  $T_0 = 0$  case, while for the experiment, it is good practice to remove the value of the ambient temperature from the captured thermal feed.

*D. Sources*

Sources in the heat equation are displayed in the inhomogeneity (nonzero) term of the equation. For this application scenario, we expect a source to be present in a disk with radius  $\rho_0$  around the origin on the  $z = 0$  surface. The source has a homogeneous distribution over this area, which models laser thermography better than the Gaussian distribution of current approaches. This is both apparent in the laser diode’s homogeneous output intensity as well as its negligible amount of divergence over the range of up to a few meters. The source should be turned on between  $t = 0$  and  $t = t_0$ , and the rate of increase in temperature in the material due to the laser source (a factor of laser power as well as surface absorptance and volumetric heat capacity of the material) is denoted by  $C$ . This value is generally dependent on the absorptivity value of the object, which is the ratio of incident electromagnetic radiation that is absorbed (as opposed to reflected or transmitted).

*E. Model*

It is possible to solve the heat equation for this application scenario with the previously discussed conditions. The problem is defined by a spatially constant nonzero initial condition, a both spatially and temporally bounded inhomogeneity term, and a boundary condition that is taken care of by infinite two-sided symmetrical extension of the previous terms.

TABLE I

SUBPROBLEM EQUATIONS AND CORRESPONDING INITIAL CONDITIONS

First Subproblem	Second Subproblem
$\frac{\partial U}{\partial t} = \alpha \Delta U$	$\frac{\partial V}{\partial t} = \alpha \Delta V + C \cdot \delta(x, y, z) \cdot (\Theta(t) - \Theta(t - t_0)) \cdot (\Theta(\rho) - \Theta(\rho - \rho_0))$
$U(x, y, z, 0) = T_0$	$V(x, y, z, 0) = 0$

The initial condition and the inhomogeneity can be accounted for in separate subproblems due to the superposition principle, which the linearity of the heat equation permits to be used. The first problem has the nonzero initial condition, but is homogeneous, i.e., there are no sources. Since the initial condition is constant in this case, it is expected that the result retains this constant temperature over time (and it is indeed verified in the Appendix). The second problem contains the source terms, but has zero initial condition. Both problems are subject to the spatial extensions in the  $z$ -direction. Table I lists the differential equations and initial conditions governing these subproblems.

The solution to the original problem is then the sum of the temperature functions acquired from these subproblems

$$T(x, y, z, t) = U(x, y, z, t) + V(x, y, z, t). \quad (1)$$

In these equations,  $\alpha$  represents the thermal diffusivity of the material, while  $t_0$  and  $\rho_0$  stand for the duration and radius of excitation, respectively.  $\delta$  indicates the Dirac-delta function and  $\Theta$  denotes the Heaviside step function. The final equation for  $V(t)$  is as follows:

$$V(t) = \iint_D \frac{C}{4\pi\alpha} \sum_{-\infty}^{\infty} \sqrt{\frac{1}{w_i^2}} \cdot \left( \operatorname{erf} \left( \sqrt{\frac{w_i^2}{4\alpha(t-t_0)}} \right) - \operatorname{erf} \left( \sqrt{\frac{w_i^2}{4\alpha t}} \right) \right) dA \quad (2)$$

In (2), the integration is performed over the disk  $D$  with radius  $\rho_0$ , where the excitation takes place.  $w_i$  denotes the distance from the point of integration to the  $i$ th image source. This is the equation that is used as the basis of the simulation in this paper, since the ambient temperature [ $U(x, y, z, t) = T_0$ ] is removed from the processed data. The full derivation of these equations is listed in the Appendix.

#### IV. ANALYSIS OF THE MODEL

##### A. Validity Analysis

A series of simulations have been carried out in MATLAB on a professional workstation to provide validation for the proposed mathematical model. In all of these simulations, an ambient temperature of  $T_0 = 0$  was assumed, therefore, only the heat spread by the source was modeled. As discussed in Section III, the superposition property of the heat equation ensures that any nonzero  $T_0$  ambient temperature would only result in adding a constant  $T_0$  term to these results (see the Appendix for proof). Therefore, these simulations can also be understood as corresponding to the temperature signal after having subtracted its initial (pre-excitation) temperature component.

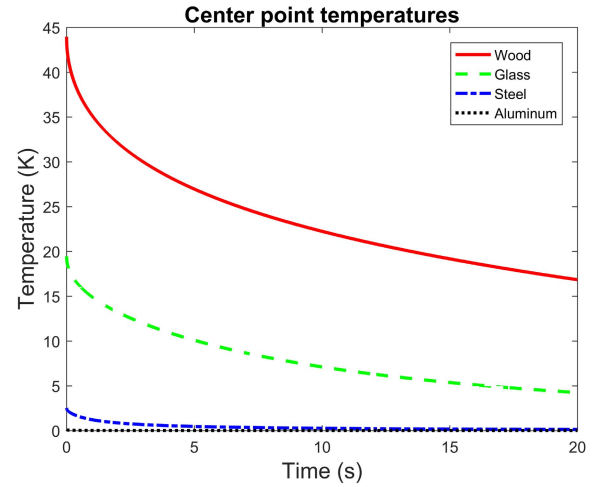


Fig. 2. Center point temperatures after 20 s of excitation.

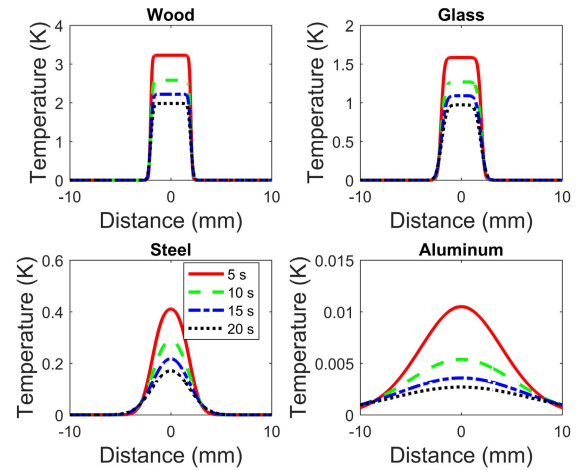


Fig. 3. Temperature distribution of materials over center line, 5 s (red), 10 s (green), 15 s (blue), and 20 s (black) after 10 s of excitation.

Fig. 2 displays temperatures at the origin (the center point of excitation) over time, starting from the time when the excitation period finishes for four materials (wood, glass, steel, and aluminum). It is visible that less diffuse materials have higher starting temperatures at their center, which is well in line with expectations based on theory. Fig. 3 shows plots of the evolution of the temperatures of four materials over the cross Section of the excitation area and its neighborhood. The lines correspond to the subsequent points in time from 0 to 20 s after excitation. It is visible that the overall thermal energy in any of these images (which is proportional to the integral of temperature) decreases over time, which is explained by thermal diffusion taking place not only along the direction of the plotted line, but also both in a perpendicular direction on the surface and toward the inside of the object.

##### B. Sensitivity Analysis

This Section explores the effects of sample thickness and the mathematical treatment of boundary conditions on the simulation results. During modeling, the Neumann-type boundary conditions were imposed on the material's surfaces to account for a lack of conductive heat transfer into and out of the

material. This was mathematically equivalent to symmetrically extending both the material and the excitation areas infinitely in both directions. As a result, the acquired formula contains the effects of sources at  $z = 2iL$ , where  $L$  is the material thickness and  $i$  represents all integers from  $-\infty$  to  $+\infty$ . In practice, however, it only makes sense to treat  $i$  values in a finite range, from  $-n$  to  $+n$ . In general, it has become validated that the more diffuse a material is, the more imaginary sources need to be taken into account. Another key observation is that for simulations where less time has passed since the end of the excitation period, a lower amount of sources were necessary to be taken into account. Following these results, we have programmed simulations to model all sources whose contribution is at least  $10^{-6}$  (one millionth) part of the overall temperature value. This ensures that the simulations stay accurate to a high degree regardless of the simulational parameters.

The second part of the analysis focuses on how the sample thickness affects the temperature distribution. It was concluded that for wood ( $\alpha = 0.082 \text{ mm}^2/\text{s}$ ), any thickness that is at least 3 mm can be considered as semi-infinite for at least 20 s, since temperature distributions remained unaffected by larger thickness values. In the case of aluminum ( $\alpha = 97 \text{ mm}^2/\text{s}$ ), this boundary is at the order of 30 mm. In general, the more diffuse a material is, the larger its "semi-infinite boundary" becomes, that is, the value above which the thickness of the sample has no effect on temperature. It can be concluded that for the presented time frame (20 s), any thickness above 30 mm can be assumed as infinite for any material, since aluminum has one of the highest thermal diffusivity values among common materials.

### C. Feature Analysis

This Section is dedicated to the analysis of two features: full width at half maximum (FWHM) and center point temperature.

1) *Full Width at Half Maximum*: The FWHM feature is defined by the following procedure. At any point in time after excitation, we first normalize the temperature image by subtracting the temperature before the excitation ( $T_0$ ). Next, we identify the maximum temperature. This maximum temperature should arise at the center of excitation. Finally, the region on the excitation plane ( $z = 0$ ) with normalized temperature that is half of the normalized temperature of the center point is identified. Given that the simulation equation exhibits circular symmetry for around the ( $x = 0, y = 0$ ) axis, this results in this being a circular region. The FWHM feature is then defined as the diameter of this circle.

In terms of the sensitivity of this feature to the excitation parameters, we have observed the following through a series of simulations.

- 1) The FWHM is always at least as large as the excitation radius, which affects the results for lower diffusivities. However, higher diffusivities have a considerably higher FWHM, making them less sensitive to changes in the excitation radius.
- 2) The spatial resolution of the simulation discretizes the FWHM. Although temperatures are calculated

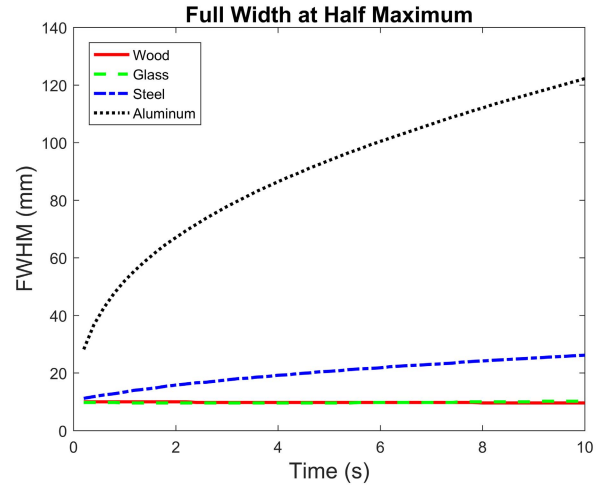


Fig. 4. FWHM of wood, glass, steel, and aluminum after 20 s of excitation.

analytically (representing the physical reality of heat transfer), they are measured with a finite resolution (representing the discrete resolution of thermal cameras). As a result, measured FWHM values are always multiples of the sampling distance and a higher resolution yields a smoother (less stepwise) FWHM curve.

2) *Center Point Temperature*: The center point temperature feature denotes the temperature at the center of excitation. It is expected that a material with lower diffusivity retains more of the excitation energy near its center, resulting in a higher center point temperature. This prediction is confirmed by the simulation, where a clear inverse proportionality is visible.

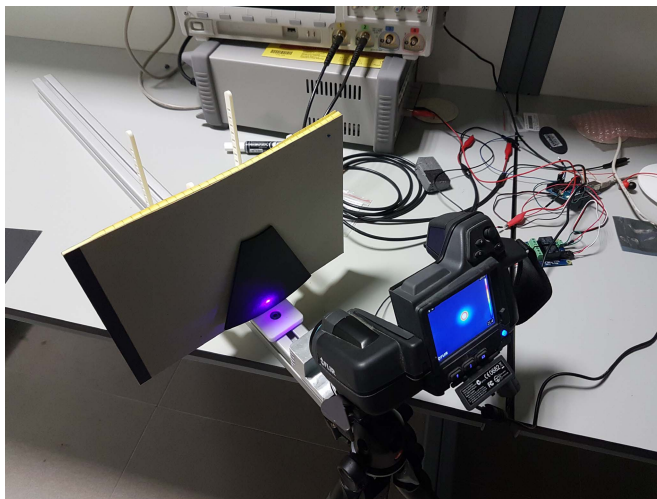
3) *Time-Domain Feature Analysis*: The evolution of the previously introduced features was also examined in the time domain. Fig. 4 represents the FWHM of wood, glass, steel, and aluminum after 20 s of excitation, while Fig. 2 shows the center point temperatures of these materials over time.

## V. EXPERIMENTAL ANALYSIS

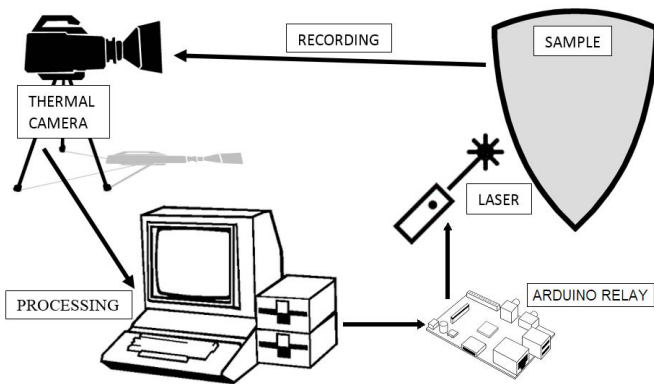
A series of experiments have been carried out based on the mathematical model. These experiments are conducted using standard laser excitation step thermography that the model represents. The procedure is described in the following sections.

### A. Experimental Setup

The experimental setup comprises a laser source, a thermal camera, a control circuit, and a material sample. A snapshot of the setup is shown in Fig. 5(a). A diagram of the components is shown in Fig. 5(b). The laser source is rated at 400 mW and emits a violet beam with a wavelength of 405 nm. The thermal camera is a FLIR450sc model, capable of  $480 \times 320$  resolution and 30 fps frame rate. The laser source is approximately 12 cm away from the surface of the sample, while the camera is approximately 20 cm away from it. The control circuit involves an Arduino board that acts as a relay switch to supply power to the laser diode and is instructed through the serial port, as well as a desktop workstation running the MATLAB R2016a and FLIR ResearchIR software [46].



(a)



(b)

Fig. 5. Modeled experiment. (a) Experimental module. (b) Diagram of the experiment.

### B. Experimental Procedure

The experimental procedure comprises of three parts: performing the experiment, processing the data, and performing the model fitting on the data. During the procedure, the laser source is turned on for 10 s, during which time it heats up the material at a specified location. Following the excitation period, the laser turns off, which marks the beginning of the cooldown phase. This cooldown is captured by a thermal camera that measures the thermal radiation emitted from the surface of the material and deduces its temperature with a known spatial resolution and frame rate. This data is used as the value that the model is fit on. In each experimental session, data acquisition lasts for approximately 16 s, during which the camera is set to record thermal data with a resolution of  $320 \times 240$  and a frame rate of 25 fps (resulting in around 400 frames in total, subject to occasional variations in the frame rate).

The acquired data is processed in a sequence of steps: In the first step, the maximum temperatures of the frames are extracted, along with their corresponding timestamps. These data points are then subjected to the removal of the ambient temperature as well as temperature spikes (rare incidences where the thermal camera measures an irreally large value for

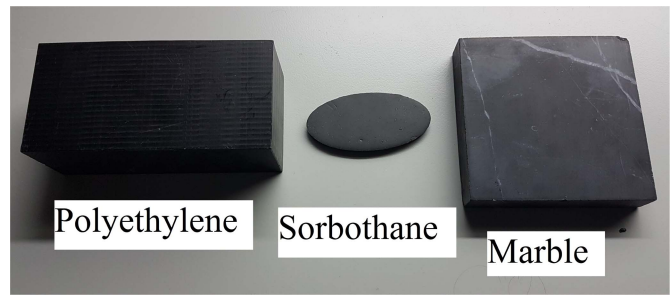


Fig. 6. Experimental samples.

a single frame - a hardware peculiarity). Since the temperature data are noisy (the equipment is rated at a noise equivalent temperature difference of 50 mK), a moving average smoothing is performed with a 5-frame window. Finally, the data is truncated so that only the initial sequence corresponding to the first 80% of cooldown (the temperature difference between the start and the end of the sequence) is kept. This is based on the fact that since the noise levels are approximately the same for the entire sequence, the higher temperature parts have a significantly better signal-to-noise ratio, and they should serve as the basis for model fitting.

Having processed the data in the above-mentioned way, the mathematical model is then fit on the acquired data. Known inputs of the model include the duration and radius of excitation, the thickness of the sample and tolerance of error. Unknown parameters include the values of  $C$  and  $\alpha$ , as these both depend on the material properties.  $C$  corresponds to the rate of increase in temperature due to the laser source, and it is based on the power of the laser diode, the surface absorptivity and the volumetric heat capacity of the material. All samples in the experiment were chosen to have a smooth black surface, implying an absorptivity value of approximately 1.  $\alpha$  is the thermal diffusivity of the material, which is the ratio of its thermal conductivity and volumetric heat capacity. Initial values for these parameters are set at 2 K/s and  $2 \text{ mm}^2/\text{s}$ , respectively. The objective function is declared as the following: we perform center point simulations with the above parameters, on the time points corresponding to the data. The difference between the simulated and measured values at each time points is calculated, squared, and summed together. The aim of the process is to find the values of  $C$  and  $\alpha$  for which this discrepancy is minimized.0

### C. Results

For this experiment, three material samples were used: Sorbothane with a durometer value of 70 on the Shore OO hardness scale, a piece of machining polyethylene and a slab of black marble. Given the smooth black surface of these materials, they can be closely approximated as black bodies, and their absorptivity was correspondingly taken as 1. All samples had width and height measurements that were more than an order of magnitude larger than the radius of the laser beam, and thus, ensured that the modeling assumptions of infinite width and height are good approximations. Fig. 6 shows these samples next to each other. They were each

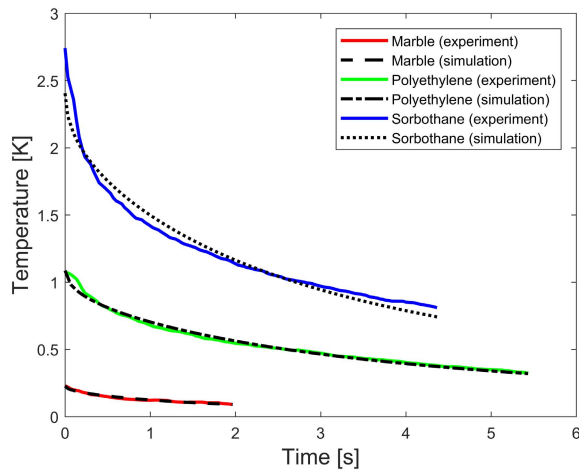


Fig. 7. Comparison of experimental and fit simulational data.

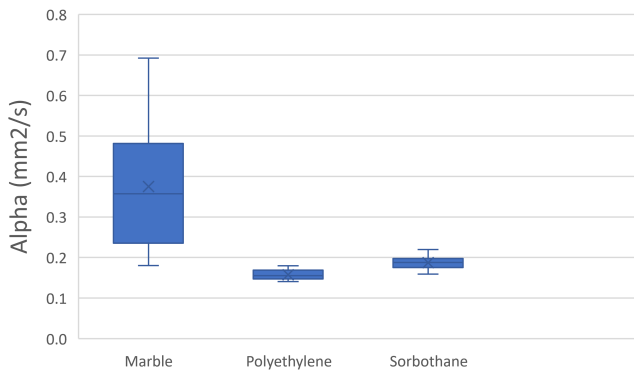


Fig. 8.  $\alpha$  values for the three materials.

examined 10 times with the procedure discussed above. For each of these cases, the values of  $C$  and  $\alpha$  were recorded. Fig. 7 shows the processed temperature data of one session for each sample, as well as the fit simulational curves.

The  $C$  and  $\alpha$  values from each of the above-mentioned sessions were plotted against each other to see whether they could serve as a basis for classification between these materials. Fig. 8 shows the box-and-whiskers diagram for the  $\alpha$  values, while Fig. 9 presents the same for the  $C$  values. Fig. 10 combines the previous two graphs and presents each data point on a 2-D plane according to these two values. It can be seen that even though the  $C$  value plot allows for sufficiently easy classification, the combined plot strengthens this approach.

*D. Discussion*

This experiment aimed to acquire a set of parameters of the samples that can be used to differentiate between them based on their thermal responses. Having presented the results of the 2-D parametric optimization-based model fitting, the result is that classification is indeed possible between these materials. However, there are a few points worthy of mentioning.

First, the nature of the optimization is dependent on the objective function, which in our case is continuous and differentiable, but cannot be written in closed form. However, analysis suggests that there exist certain parametric (close

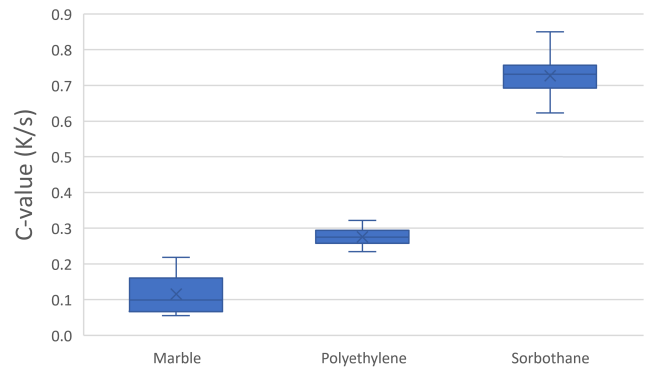


Fig. 9.  $C$  values for the three materials.

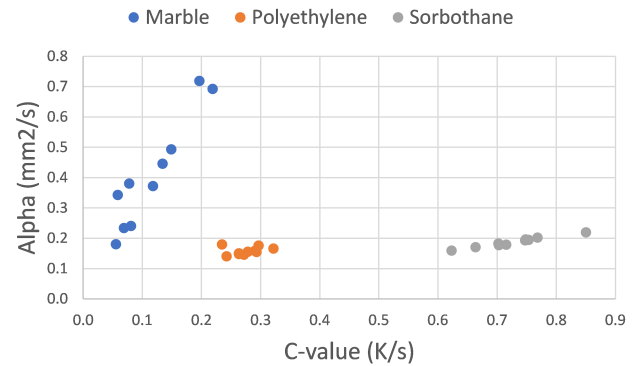


Fig. 10.  $\alpha$  and  $C$  values for the three materials, combined.

to proportional) relations between  $\alpha$  and  $C$  values, along which the simulation changes its values very slowly. In other words, it means that the modeled curve for a material with high diffusivity heated strongly will bear similarity that of a material with lower diffusivity that was heated less. This is a challenge, particularly since while in theory there should be enough difference to differentiate between these cases, in reality the noise level limits this ability. The marble (blue) point cloud in Fig. 10 exemplifies this relationship. It also makes sense for marble to have the largest spread, as its relatively low maximum temperature values (seen in Fig. 7) are a result of its higher thermal diffusivity.

Despite the above-mentioned challenge, these two parameters must remain as unknown values in the simulation, for they are both dependent on the material composition of the samples, which is the fundamental unknown component of the experiment. However, these parameters are not independent. In fact, by theory, their ratio should be proportional to the thermal conductivity of the material. In this case, we see that all the three point clouds on Fig. 10 have a roughly linear pattern with different slopes. Marble has the highest slope, which corresponds well with the fact that it has a higher thermal conductivity than plastic and polyurethane (the main component of Sorbothane).

During the simulation and model fitting phases, we have assumed that the material is homogeneous with respect to the thermal parameters used. However, the sensitivity analysis has demonstrated that depending on the diffusivity of the material,

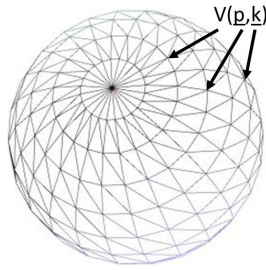


Fig. 11. Polygonal thermal model of the surface of an object. Each point  $V$  in the mesh encodes position information ( $p$ ) and thermal properties ( $k$ ).

and considering short enough measurement durations, this condition may be relaxed in favor of a local homogeneity condition. This could allow for objects with several material components on their surface to be mapped to a discrete polygonal thermal model that contains nodes at different positions of measurement with the corresponding thermal properties at those locations, as illustrated in Fig. 11.

It is also worth noting that all materials in the simulations were treated as black bodies with smooth surface. This is identical to the experimental samples. Such objects have emissivity and absorptivity that are close to 1, meaning that they absorb most of the incident light, as opposed to transmitting or reflecting it. In addition, most thermal cameras do emissivity compensation on their own (based on the spectral response of the IR camera as well as a separate RGB camera), which is usually reliable. Therefore, the data we acquire from the thermal camera is not electromagnetic radiation intensity, but temperature calculated by the camera based on the emissivity value of the target. In theory, most objects with sufficiently matte surfaces can be subject to thermographic inspection.

Since this paper presents a new research that has no direct precedent in the field, there are a number of experimental parameters that had to be decided on without the guidance of the previous research results. These include the power supplied by the laser diode, the length of excitation, the set of features in the heat signature selected for inspection, and the methods of processing the data. A number of arguments have been taken into account when deciding on these parameters. For example, a lower amount of laser power results in lower signal-to-noise ratio, which yields degraded results. On the other hand, a higher power laser would be less suitable for delicate materials, thereby reducing the range of potential applications. Similarly, given a fixed laser power, a short excitation window means less energy is deposited into the material, resulting in a smaller difference in temperature between the excitation region and its surrounding area. Conversely, increasing the excitation window beyond a certain amount of time would simply mean that a larger part of the excitation is allowed to spread out before the excitation ends—and before recording begins. This issue is especially relevant for materials with higher thermal diffusivity values, which are also the ones that are bound to have the lower signal-to-noise ratio anyway. Therefore, it might be a more suitable approach to drop a fixed set of values in favor of an adaptive algorithm with respect to these parameters, where an initial measurement would determine the

parameters to be used in a followup measurement that has higher accuracy and precision.

Finally, it is worth talking about advective air currents. We have assumed no heat exchange between the surface of the material and the environment, but in reality heat is indeed taken away by air currents. However, our reasoning is that the rate at which this phenomena is taking place is sufficiently slow that it does not affect the experiment significantly. Using the numerical values detailed by [47], the rate of energy dissipation through advection over the very small excitation area ( $\approx 10^{-4}m^2$ ) results in a loss of less than 1% of the power supplied by the laser. For this reason, it can be concluded that advection is small enough that its effect can be neglected.

## VI. CONCLUSION

Our results show that in multiple cases, it is certainly possible to classify material using thermal properties. This experiment lays down the groundwork for developing an efficient and effective thermal characterization method.

There are a number of objectives worth pursuing in the future. First, we plan to examine the proposed model on a wide spectrum of material with varying thermal properties, as well investigate the possibility of classification between a range of different alloys. Optimization of all experimental parameters, as discussed in Section V, is also to be performed. Furthermore, machine learning algorithms will be utilized to derive physical properties from the measured thermal properties. This has the potential to enable the proposed model to indirectly measure the physical properties of materials without physical contact. Potential applications for measuring the physical properties include haptic modeling, human-robot interaction, and teleoperation systems.

## APPENDIX

### DERIVATION OF THE SIMULATED FORMULA FROM THE HEAT EQUATION

#### A. Solution to the Nonzero Initial Condition Problem

For this subproblem we need to find  $U(x, y, z, t)$ , such that

$$\frac{\partial U}{\partial t} = \alpha \Delta U \quad (3)$$

$$\forall(x, y, z): U(x, y, z, 0) = T_0 \quad (4)$$

In the above form,  $\alpha$  represents thermal diffusivity or the ratio of thermal conductance and volumetric heat capacity. The solution formula to this problem is as follows:

$$\begin{aligned} U(x, y, z, t) &= \left( \frac{1}{\sqrt{4\pi\alpha t}} \right)^3 \iiint_{-\infty}^{\infty} e^{-\frac{(x-a)^2+(y-b)^2+(z-c)^2}{4\alpha t}} T_0 da db dc. \end{aligned} \quad (5)$$

Using the substitutions:  $f = x - a$ ,  $g = y - b$  and  $h = z - c$ , we get

$$U(x, y, z, t) = \left( \frac{1}{\sqrt{4\pi\alpha t}} \right)^3 \iiint_{-\infty}^{\infty} e^{-\frac{f^2+g^2+h^2}{4\alpha t}} T_0 df dg dh. \quad (6)$$



Separating the independent terms leads to

$$U(x, y, z, t) = \left( \frac{1}{\sqrt{4\pi\alpha t}} \right)^3 T_0 \int_{-\infty}^{\infty} e^{-\frac{f^2}{4\alpha t}} df \int_{-\infty}^{\infty} e^{-\frac{g^2}{4\alpha t}} dg \int_{-\infty}^{\infty} e^{-\frac{h^2}{4\alpha t}} dh. \quad (7)$$

These separate integrals are trivial to solve using scaled substitutions and the result is

$$U(x, y, z, t) = \left( \frac{1}{\sqrt{4\pi\alpha t}} \right)^3 T_0 (\sqrt{\pi \cdot 4\alpha t})^3 = T_0. \quad (8)$$

As visible, the result for this subproblem is in line with the above detailed expectations, i.e., a constant temperature field due to the initial conditions.

### B. Solution to the Inhomogeneous Problem

For this subproblem, we first aim to find  $V'(x, y, z, t)$ , such that

$$\frac{\partial V'}{\partial t} = \alpha \Delta V' + C \cdot \delta(x, y, z) \cdot (\Theta(t) - \Theta(t - t_0)) \quad (9)$$

$$\forall(x, y, z): V'(x, y, z, 0) = 0. \quad (10)$$

This subproblem so far only supposes a point source as opposed to a spatially elongated (disk shaped) one, so there is an additional need for convolution of this  $V'$  with respect to the source distribution, to form  $V$  before combining it with  $U$ . However, it is better in terms of visibility to solve first for a point source. The  $\Theta$  function represents the Heaviside step function, accounting for the duration of excitation. The solution formula to this problem is as follows:

$$V'(x, y, z, t) = \int_{s=0}^t \iiint_{-\infty}^{\infty} \left( \frac{1}{\sqrt{4\pi\alpha(t-s)}} \right)^3 e^{-\frac{(x-a)^2 + (y-b)^2 + (z-c)^2}{4\alpha(t-s)}} \cdot C \cdot \sum_{i=-\infty}^{\infty} \delta(a, b, c - 2iL) \cdot (\Theta(s) - \Theta(s - t_0)) da db dc ds. \quad (11)$$

Using the sifting property of the Dirac-delta function, (11) simplifies to

$$V'(x, y, z, t) = \int_{s=0}^t \int_{z=-\infty}^{\infty} \left( \frac{1}{\sqrt{4\pi\alpha(t-s)}} \right)^3 e^{-\frac{x^2 + y^2 + (z-c)^2}{4\alpha(t-s)}} \cdot C \cdot \sum_{i=-\infty}^{\infty} \delta(c - 2iL) \cdot (\Theta(s) - \Theta(s - t_0)) dc ds \quad (12)$$

$$V'(x, y, z, t) = \int_{s=0}^t \left( \frac{1}{\sqrt{4\pi\alpha(t-s)}} \right)^3 \sum_{i=-\infty}^{\infty} e^{-\frac{x^2 + y^2 + (z-2iL)^2}{4\alpha(t-s)}} \cdot C \cdot (\Theta(s) - \Theta(s - t_0)) ds. \quad (13)$$

From this point, let  $d_i^2$  denotes  $x^2 + y^2 + (z - 2iL)^2$ , which is the distance of the point with coordinates  $(x, y, z)$  from the  $i$ th image source. It is now possible to demonstrate how the

step function affects the integration limits with respect to time. For  $0 < t < t_0$  (during excitation)

$$V'(x, y, z, t) = \int_{s=0}^t \left( \frac{1}{\sqrt{4\pi\alpha(t-s)}} \right)^3 \sum_{i=-\infty}^{\infty} C \cdot e^{-\frac{d_i^2}{4\alpha(t-s)}} ds. \quad (14)$$

For  $t > t_0$  (after excitation)

$$V'(x, y, z, t) = \int_{s=0}^{t_0} \left( \frac{1}{\sqrt{4\pi\alpha(t-s)}} \right)^3 \sum_{i=-\infty}^{\infty} C \cdot e^{-\frac{d_i^2}{4\alpha(t-s)}} ds. \quad (15)$$

The more useful equation out of these two is the second one, since postexcitation temperature measurements are generally more reliable than those during excitation. Therefore, from this point onward, we assume  $t > t_0$ .

It is possible to bring the summation outside of the integration, resulting in

$$V'(x, y, z, t) = C \cdot \sum_{i=-\infty}^{\infty} \int_{s=0}^{t_0} \left( \frac{1}{\sqrt{4\pi\alpha(t-s)}} \right)^3 e^{-\frac{d_i^2}{4\alpha(t-s)}} ds = C \cdot \sum_{i=-\infty}^{\infty} S_i. \quad (16)$$

Examining a single term  $S_i$

$$S_i = \int_{s=0}^{t_0} \left( \frac{1}{\sqrt{4\pi\alpha(t-s)}} \right)^3 e^{-\frac{d_i^2}{4\alpha(t-s)}} ds. \quad (17)$$

Using substitutions:  $c_1 = (1/(4\pi\alpha))^{1/2}$ ,  $c_2 = d_i^2/4\alpha$ ,  $w = t - s$ , we get a simpler integral that is easier to solve

$$S_i = c_1 \int_{w=t-t_0}^t \left( \frac{1}{\sqrt{w}} \right)^3 e^{-\frac{c_2}{w}} dw = c_1 \left[ -\sqrt{\frac{\pi}{c_2}} \cdot \operatorname{erf} \left( \sqrt{\frac{c_2}{w}} \right) \right]_{w=t-t_0}^{w=t}. \quad (18)$$

Substituting back the original parameters, we get

$$S_i = \left( \frac{1}{\sqrt{4\pi\alpha}} \right)^3 \left[ -\sqrt{\frac{4\alpha\pi}{d_i^2}} \cdot \operatorname{erf} \left( \sqrt{\frac{d_i^2}{4\alpha w}} \right) \right]_{w=t-t_0}^{w=t}. \quad (19)$$

This simplifies to

$$S_i = \left( \frac{1}{4\pi\alpha} \right) \left[ -\sqrt{\frac{1}{d_i^2}} \cdot \operatorname{erf} \left( \sqrt{\frac{d_i^2}{4\alpha w}} \right) \right]_{w=t-t_0}^{w=t}. \quad (20)$$

Therefore, we get

$$S_i = \left( \frac{1}{4\pi\alpha} \right) \sqrt{\frac{1}{d_i^2}} \cdot \left( \operatorname{erf} \left( \sqrt{\frac{d_i^2}{4\alpha(t-t_0)}} \right) - \operatorname{erf} \left( \sqrt{\frac{d_i^2}{4\alpha t}} \right) \right) \quad (21)$$

$$V'(x, y, z, t) = \frac{C}{4\pi\alpha} \sum_{i=-\infty}^{\infty} \sqrt{\frac{1}{d_i^2}} \cdot \left( \operatorname{erf} \left( \sqrt{\frac{d_i^2}{4\alpha(t-t_0)}} \right) - \operatorname{erf} \left( \sqrt{\frac{d_i^2}{4\alpha t}} \right) \right). \quad (22)$$

1) *Accounting for Distribution of Excitation:* The previous result for  $V'(x, y, z, t)$  holds for an excitation that is incident on  $(x, y, z) = (0, 0, 0)$ , i.e., on a single point on the surface. However, it is more realistic to model excitation as incident on a disk with radius  $r_0$  in the  $xy$  plane around the origin. In order to account for this, we need to convolve  $V'$  in the spatial domain with a function that gives 1 inside the excitation area and 0 outside of it. Such a function  $k(x, y, z)$  can be written as  $k(x, y, z) = (1 - \Theta(\sqrt{x^2 + y^2} - r_0)) \cdot \delta(z)$ . The convolution then becomes

$$V(x, y, z, t) = \iiint_{-\infty}^{\infty} V'(x - k, y - m, z - n, t) \cdot (1 - \Theta(\sqrt{k^2 + m^2} - r_0)) \cdot \delta(n) dn dm dk \quad (23)$$

$$V(x, y, z, t) = \iint_{-\infty}^{\infty} V'(x - k, y - m, z, t) \cdot (1 - \Theta(\sqrt{k^2 + m^2} - r_0)) dm dk. \quad (24)$$

Performing the appropriate changes in the domain that are dictated by the step function gives the following expression:

$$V(x, y, z, t) = \int_{k=-r_0}^{r_0} \int_{m=-\sqrt{r_0^2 - k^2}}^{\sqrt{r_0^2 - k^2}} V'(x - k, y - m, z, t) dm dk. \quad (25)$$

Therefore,

$$V(x, y, z, t) = \int_{k=-r_0}^{r_0} \int_{m=-\sqrt{r_0^2 - k^2}}^{\sqrt{r_0^2 - k^2}} \frac{C}{4\pi\alpha} \sum_{-\infty}^{\infty} \sqrt{\frac{1}{v_i^2}} \cdot \left( \operatorname{erf} \left( \sqrt{\frac{v_i^2}{4\alpha(t - t_0)}} \right) - \operatorname{erf} \left( \sqrt{\frac{v_i^2}{4\alpha t}} \right) \right) dm dk. \quad (26)$$

Here,  $v_i^2 = (x - k)^2 + (y - m)^2 + (z - 2il)^2$  denotes the distance from the point of integration to the  $i$ th image source. At the center point  $((x, y, z) = (0, 0, 0))$ , this takes the following form as the modeled equation [using  $w_i^2 = k^2 + m^2 + (2il)^2$ ]:

$$V(t) = \int_{k=-r_0}^{r_0} \int_{m=-\sqrt{r_0^2 - k^2}}^{\sqrt{r_0^2 - k^2}} \frac{C}{4\pi\alpha} \sum_{-\infty}^{\infty} \sqrt{\frac{1}{w_i^2}} \cdot \left( \operatorname{erf} \left( \sqrt{\frac{w_i^2}{4\alpha(t - t_0)}} \right) - \operatorname{erf} \left( \sqrt{\frac{w_i^2}{4\alpha t}} \right) \right) dm dk. \quad (27)$$

## REFERENCES

- [1] M. Benali-Khouldjal, M. Hafez, J.-M. Alexandre, J. Benachour, and A. Kheddar, "Thermal feedback model for virtual reality," in *Proc. Int. Symp. Micromechatronics Human Sci. (IEEE Cat)*, Oct. 2003, pp. 153–158.
- [2] M. Bergamasco, A. A. Alessi, and M. Calcara, "Thermal feedback in virtual environments," *Presence, Teleoper. Virtual Environ.*, vol. 6, no. 6, pp. 617–629, 1997.
- [3] X. Maldague, *Theory and Practice of Infrared Technology for Nondestructive Testing*. New York, NY, USA: Wiley, 2001.
- [4] V. Yefremenko *et al.*, "A broadband imaging system for research applications," *Rev. Sci. Instrum.*, vol. 80, May 2009, Art. no. 056104.
- [5] T. Durrani, A. Rauf, K. Boyle, F. Lotti, and S. Baronti, "Thermal imaging techniques for the non destructive inspection of composite materials in real-time," in *Proc. IEEE Int. Conf. Acoust., Speech Signal Process. (ICASSP)*, Apr. 1987, pp. 598–601.
- [6] T. S. Durrani, A. Rauf, K. Boyle, and F. Lotti, "Reconstruction techniques for the inspection of composite materials using thermal images," in *Proc. Int. Conf. Acoust., Speech Signal Process. (ICASSP)*, 1988, pp. 863–866.
- [7] T. Kakuda, A. Limarga, A. Vaidya, A. Kulkarni, and T. D. Bennett, "Non-destructive thermal property measurement of an APS TBC on an intact turbine blade," *Surf. Coat. Technol.*, vol. 205, no. 2, pp. 446–451, 2010.
- [8] P. Bison, F. Cernushi, and S. Capelli, "A thermographic technique for the simultaneous estimation of in-plane and in-depth thermal diffusivities of TBCs," *Surf. Coat. Technol.*, vol. 205, no. 10, pp. 3128–3133, 2011.
- [9] F. Cernushi, P. Bison, S. Marinetti, and E. Campagnoli, "Thermal diffusivity measurement by thermographic technique for the non-destructive integrity assessment of TBCs coupons," *Surf. Coat. Technol.*, vol. 205, no. 2, pp. 498–505, 2010.
- [10] S. E. Burrows, S. Dixon, S. G. Pickering, T. Li, and D. P. Almond, "Thermographic detection of surface breaking defects using a scanning laser source," *NDT E Int.*, vol. 44, no. 7, pp. 589–596, 2011.
- [11] I. Plotog *et al.*, "Methods for pads thermophysical parameters assessment in terms of 4P soldering model," in *Proc. IEEE 34th Int. Spring Seminar Electron. Technol.*, 2011, pp. 320–326.
- [12] N. Horny, J.-F. Henry, S. Offerman, C. Bissieux, and J. L. Beaudoin. (Oct. 6, 2016). *Photothermal Infrared Thermography Applied to the Identification of Thin Layer Thermophysical Properties*. [Online]. Available: <https://www.researchgate.net/publication/265667818>
- [13] N. W. Pech-May, A. Oleaga, A. Mendioroz, and A. Salazar, "Fast characterization of the width of vertical cracks using pulsed laser spot infrared thermography," *J. Nondestruct. Eval.*, vol. 35, Jun. 2016, Art. no. 22.
- [14] S. E. Burrows, A. Rashed, D. P. Almond, and S. Dixon, "Combined laser spot imaging thermography and ultrasonic measurements for crack detection," *Nondestruct. Test. Eval.*, vol. 22, nos. 2–3, pp. 217–227, Feb. 2007.
- [15] S. Huth, O. Breitenstein, A. Huber, D. Dantz, U. Lambert, and F. Altmann, "Lock-in IR-thermography—A novel tool for material and device characterization," *Solid State Phenom.*, vols. 82–84, pp. 741–746, Nov. 2002.
- [16] P. E. Raad, P. L. Komarov, and M. G. Burzo, "Non-contact surface temperature measurements coupled with ultrafast real-time computation," in *Proc. 23rd Annu. IEEE Semiconductor Thermal Meas. Manage. Symp.*, Mar. 2007, pp. 57–63.
- [17] C. Ionescu, M. Brânzei, B. Mihailescu, and D. Bonfert, "Studies on thermal properties of substrates for electronics using IR thermography," in *Proc. IEEE 20th Int. Symp. Design Technol. Electron. Packag. (SIITME)*, Oct. 2014, pp. 45–49.
- [18] J.-L. Bodnar, J.-L. Nicolas, K. Mouhoubi, and V. Detalle, "Stimulated infrared thermography applied to thermophysical characterization of cultural heritage mural paintings," *Eur. Phys. J. Appl. Phys.*, vol. 60, no. 2, 2012, Art. no. 21003.
- [19] M. Kamel, J.-L. Bodnar, V. Detalle, and J.-M. Vallet, "Stimulated infrared thermography applied to the local characterization of fresco," in *Proc. Quant. Infr. Thermography Conf. (QIRT)*, 2016, pp. 135–143.
- [20] K. Mouhoubi, J.-L. Bodnar, V. Detalle, and J.-M. Vallet, "Non-destructive testing of works of art by stimulated by infrared thermography: PPT interest," in *Proc. Quant. Infr. Thermography Conf. (QIRT)*, 2016, pp. 144–151.
- [21] J.-L. Bodnar, J.-L. Nicolas, K. Mouhoubi, J. C. Candore, and V. Detalle, "Characterization of an inclusion of plastazote located in an academic fresco by photothermal thermography," *Int. J. Thermophys.*, vol. 34, nos. 8–9, pp. 1633–1637, 2013.
- [22] R. Usamentiaga, P. Venegas, J. Guerediaga, L. Vega, J. Molleda, and F. G. Bulnes, "Infrared thermography for temperature measurement and non-destructive testing," *Sensors*, vol. 14, no. 7, pp. 12305–12348, 2014.
- [23] J.-C. Krapez, L. Spagnolo, M. Friess, H.-P. Maier, and G. Neuer, "Measurement of in-plane diffusivity in non-homogeneous slabs by applying flash thermography," *Int. J. Thermal Sci.*, vol. 43, no. 10, pp. 967–977, 2004.
- [24] F. Lakestani, A. Salemo, and A. Volcan, "Modulated spot heating for the measurement of thermal diffusivity," *J. Appl. Phys.*, vol. 97, Dec. 2004, Art. no. 013704.

- [25] H. Dong, B. Zheng, and F. Chen, "Infrared sequence transformation technique for *in situ* measurement of thermal diffusivity and monitoring of thermal diffusion," *Infr. Phys. Technol.*, vol. 73, pp. 130–140, Nov. 2015.
- [26] N. W. Pech-May, A. Mendioroz, and A. Salazar, "Simultaneous measurement of the in-plane and in-depth thermal diffusivity of solids using pulsed infrared thermography with focused illumination," *NDT E Int.*, vol. 77, pp. 28–34, Jan. 2016.
- [27] S. N. Pandya *et al.*, "Calibration of a thin metal foil for infrared imaging video bolometer to estimate the spatial variation of thermal diffusivity using a photo-thermal technique," *Rev. Sci. Instrum.*, vol. 85, no. 5, 2014, Art. no. 054902.
- [28] T. Groerer, R. Phillips, and P. Rossi, "Thermal diffusivity imaging," *Amer. J. Phys.*, vol. 83, no. 11, pp. 923–927, 2015.
- [29] L. Yeshurun and H. Azhari, "Non-invasive measurement of thermal diffusivity using high-intensity focused ultrasound and through-transmission ultrasonic imaging," *Ultrasound Med. Biol.*, vol. 42, no. 1, pp. 243–256, 2016.
- [30] M. Guiatni and A. Kheddar, "Theoretical and experimental study of a heat transfer model for thermal feedback in virtual environments," in *Proc. IEEE/RSJ Int. Conf. Intell. Robots Syst.*, Nice, France, Sep. 2008, pp. 2996–3001, 2008.
- [31] L. A. Jones and H.-N. Ho, "Warm or cool, large or small? The challenge of thermal displays," *IEEE Trans. Haptics*, vol. 1, no. 1, pp. 53–70, Jun. 2008.
- [32] L. A. Jones and H.-N. Ho, "Warm or cool, large or small? The challenge of thermal displays," *IEEE Trans. Haptics*, vol. 1, no. 1, pp. 53–70, Jan. 2008. [Online]. Available: <https://dl.acm.org/citation.cfm?id=1449677>
- [33] D. G. Caldwell, N. Tsagarakis, and A. Wardle, "Mechano thermo and proprioceptor feedback for integrated haptic feedback," in *Proc. IEEE Int. Conf. Robot. Autom. (ICRA)*, vol. 3, Apr. 1997, pp. 2491–2496.
- [34] H. Ho and L. A. Jones, "Material identification using real and simulated thermal cues," in *Proc. 26th Ann. Int. Conf. IEEE Eng. Med. Biol. Soc. (EMBS)*, Sep. 2004, pp. 2462–2465.
- [35] S. Ino *et al.*, "A tactile display for presenting quality of materials by changing the temperature of skin surface," in *Proc. IEEE Int. Workshop Robot Human Commun. (ROMAN)*, Nov. 1993, pp. 220–224.
- [36] A. Yamamoto, B. Cros, H. Hasegawa, and T. Higuchi, "Control of thermal tactile display based on prediction of contact temperature," in *Proc. IEEE Int. Conf. Robot. Autom. (ICRA)*, May 2004, pp. 1536–1541.
- [37] L. Fortuna, M. Frasca, and G. M. Rivituso, "An innovative method for thermal characterization of automotive electronic devices based on CNNs," *IEEE Trans. Instrum. Meas.*, vol. 59, no. 6, pp. 1671–1677, Jun. 2010.
- [38] A. Foudazi, C. A. Edwards, M. T. Ghasr, and K. M. Donnell, "Active microwave thermography for defect detection of CFRP-strengthened cement-based materials," *IEEE Trans. Instrum. Meas.*, vol. 65, no. 11, pp. 2612–2620, Nov. 2016.
- [39] L. Cheng and G. Y. Tian, "Transient thermal behavior of eddy-current pulsed thermography for nondestructive evaluation of composites," *IEEE Trans. Instrum. Meas.*, vol. 62, no. 5, pp. 1215–1222, May 2013.
- [40] F. Maier and B. G. Zagar, "Measurement of paint coating thickness by thermal transient method," *IEEE Trans. Instrum. Meas.*, vol. 58, no. 6, pp. 1958–1966, Jun. 2009.
- [41] L. A. Jones and M. Berris, "Material discrimination and thermal perception," in *Proc. 11th Symp. Haptic Inter. Virtual Environ. Teleoper. Syst. (HAPTICS)*, 2003, pp. 171–178.
- [42] B. Deml, A. Mihalyi, and G. Hannig, "Development and experimental evaluation of a thermal display," in *Proc. 6th Int. Conf. EuroHapt.*, 2006, pp. 153–158. [Online]. Available: <http://ieeexplore.ieee.org/document/1249925/>
- [43] H.-N. Ho and L. A. Jones, "Thermal model for hand-object interactions," in *Proc. Symp. Haptic Interfaces Virtual Environ. Teleoper. Syst.*, 2006, pp. 461–467.
- [44] H.-N. Ho and L. A. Jones, "Infrared thermal measurement system for evaluating model-based thermal displays," in *Proc. 2nd Joint EuroHapt. Conf. Symp. Haptic Interfaces Virtual Environ. Teleoper. Syst. (WHC)*, Tsukuba, Japan, 2007, pp. 157–163.
- [45] (Oct. 12, 2016). *Nonhomogeneous Heat Equation, EqWorld Mathematical Equations*. [Online]. Available: <http://eqworld.ipmnet.ru/en/solutions/lpde/lpde102.pdf>
- [46] (Nov. 2, 2016). *FLIR ResearchIR Software: IR Camera Control & Analysis Software, FLIR Systems*. [Online]. Available: <http://www.flir.com/researchir/>
- [47] Michigan Technological University. (Jun. 22, 2017). *Typical Convection Coefficients to Estimate Thermal Transfer*. [Online]. Available: <http://www.me.mtu.edu/microweb/GRAPH/Intro/film.htm>



**Tamas Aujeszky** received the B.S., M.S., and Ph.D. degrees in electrical engineering from New York University, Abu Dhabi, Abu Dhabi, United Arab Emirates.

His current research interests include haptic mapping, machine learning, and image processing.



**Georgios Korres** received the degree in applied mathematics from the School of Science and Engineering, University of Crete, Crete, Greece.

He was involved in the development of educational software and hardware regarding educational robotics, and industrial automation (mainly in the field of recycling industry). His current research interests include the development of new sensors and actuators as well as the use of these in human-computer interaction.



**Mohamad Eid** received the Ph.D. degree in electrical and computer engineering from the University of Ottawa, Ottawa, ON, Canada, in 2010.

He was a Teaching and Research Associate with the University of Ottawa from 2008 to 2012. He is currently an Assistant Professor of electrical and computer engineering with the Engineering Division, New York University Abu Dhabi, Abu Dhabi, United Arab Emirates. He has co-authored the book *Haptics Technologies: Bringing Touch to Multimedia* (Springers 2011). His current research interests include multimedia haptics, with a focus on affective haptics, tangible human-computer interaction, and instrumentations (sensors and actuators).

Dr. Eid was the Co-Chair of the 3rd International IEEE Workshop on Multimedia Services and Technologies for E-health in 2013. He was involved in the organization of the Haptic-Audio-Visual Environment and Gaming workshop for the years 2007, 2008, 2009, 2010, and 2013.